

Online-CPD-coupled large-eddy simulation of pulverized-coal pyrolysis in a hot turbulent nitrogen jet

Kaidi Wan^{1,2,3}, Jun Xia^{1,2}, Zhihua Wang^{3,*}, Luiz C. Wrobel¹, Kefa Cen³

1. Department of Mechanical, Aerospace and Civil Engineering, Brunel University London, Uxbridge UB8 3PH, UK

2. Institute of Energy Futures, Brunel University London, Uxbridge UB8 3PH, UK

3. State Key Laboratory of Clean Energy Utilization, Zhejiang University, Hangzhou 310027, China

* Corresponding author: wangzh@zju.edu.cn

Abstract

The pyrolysis characteristics of pulverized-coal particles in a hot turbulent nitrogen jet were investigated using large-eddy simulation (LES). In the present study an advanced pyrolysis model, the chemical percolation devolatilization (CPD) model, has been incorporated into LES in real time. The simulation results of the developed online-CPD-coupled LES were used to calibrate the kinetic parameters of the conventional single first-order reaction model (SFOM). Through the comparison between the CPD-coupled LES and the LES using the SFOM model, the CPD-coupled LES approach is found to be able to give a better prediction on particle pyrolysis in the high-temperature turbulent flow. Finally, the effects of important parameters,

including the particle diameter, coal type, coal-feeding rate, carrier-phase velocity, and pyrolysis temperature, on the pulverized-coal pyrolysis process were investigated through parametric studies using the online-CPD-coupled LES method.

Keywords: Large-eddy simulation; Chemical percolation devolatilization; Pulverized-coal; Pyrolysis

Introduction

As a major energy source, coal has been widely utilized in power plants using the pulverized-coal combustion (PCC) technology (Cheng et al., 2015; Hashimoto et al., 2012; Liu and He, 2015; Ströhle et al., 2014; Xu et al., 2015; Zhao and Haworth, 2014). On the other hand, coal is the most polluting fossil fuel. Due to increasing environmental concerns, development of clean coal technologies, e.g., low NO_x combustion (Kuang et al., 2014; Lv et al., 2010) and oxy-coal combustion for carbon capture and storage (CCS) (Bu et al., 2015), becomes more and more important. To develop clean coal technologies, a comprehensive understanding of pulverized-coal combustion physics is necessary. Advanced laser diagnostics, which has been widely employed in gas combustion research, is usually difficult to be applied in PCC boilers due to the poor optical access of industrial furnaces (Stein et al., 2013). On the numerical side, the Reynolds-Averaged Navier-Stokes (RANS) approach is still the current industrial standard for the simulation and

modeling of the turbulent multiphase reacting flow in industrial coal-fired furnaces (Al-Abbas et al., 2013; Bermúdez et al., 2011; Hashimoto et al., 2012; Stöllinger et al., 2013; Vascellari et al., 2013a; Vascellari and Cau, 2012; Zhao and Haworth, 2014). Although having been useful in providing an estimation of the mean flow and scalar fields, this approach cannot accurately predict the turbulent fuel/air mixing, turbulent combustion and their local, unsteady interactions, since all turbulent scales are modeled in RANS (Jiang et al., 2010). Alternatively, high-fidelity simulation techniques, such as Large-eddy simulation (LES), have appeared as an effective tool for understanding complex PCC phenomena as the sustained sharp increase of computing capacity continues (Vascellari et al., 2013a).

LES has been widely employed in recent numerical PCC studies since its first use (Kurose and Makino, 2003). Kurose et al. (2009), Edge et al. (2011), Gharebaghi et al. (2011) and Chen and Ghoniem (2012) performed LES of pulverized-coal combustion in relatively large coal-fired facilities and compared their LES results with RANS and experimental ones. These studies have demonstrated that LES could give more accurate predictions of turbulent flow, combustion chemistry and their interactions in PCC. Recently, PCC-LES studies have been mainly focused on laboratory-scale pulverized-coal jet flames. Yamamoto et al. (2011) applied LES to a pulverized-coal jet flame ignited by a preheated gas flow and compared the simulation results with the experimental data (Taniguchi et al., 2001) on the flame lift-off height, gas temperature and char

burnout. The same pulverized-coal jet flame was also investigated by Pedel et al. (2012) using LES combined with the direct quadrature method of moments (DQMOM), where the particle phase was tracked in an Eulerian framework. Another laboratory-scale pulverized-coal jet flame stabilized with a methane pilot flame (Hwang et al., 2005) has also been extensively studied with PCC-LES, e.g. by Stein et al. (2013) and Franchetti et al. (2013). The velocity field statistics of the LESs agreed well with the experimental data, but the notable disagreement of the scalar statistics illustrated the complexity of modeling coal combustion in a turbulent flow. Very recently, Rabacal et al. (2015) performed massively parallel LES of pulverized-coal swirling jet flames in a large-scale laboratory furnace and a good agreement with measurements was obtained on statistics of temperature and major species.

The combustion of coal has three main stages: pyrolysis, volatile combustion and char combustion. As the first stage, the pyrolysis process has a significant influence on the kinetics of coal combustion and largely determines the combustion characteristics in the next two stages. Most numerical simulations of PCC use a conventional simplified pyrolysis model, i.e., the classical single first-order reaction model (SFOM) proposed by Badzioch and Hawksley (1970), to save computational cost (Stein et al., 2013). However, the kinetic parameters in this empirical model can vary remarkably with the coal type and the heating rate. Directly using the values for reaction parameters from technical literature can result in unacceptable errors (Vascellari et al.,

2013a). To address this problem, a method of calibrating the conventional SFOM pyrolysis model with the chemical percolation devolatilization (CPD) model (Fletcher et al., 1992; Grant et al., 1989) has been popularly adopted in recent PCC-LES studies (Franchetti et al., 2013; Rabacal et al., 2015; Stein et al., 2013; Vascellari et al., 2013b), where the CPD model was coupled with the LES solver in an offline way. As a sophisticated network pyrolysis model, the CPD model is one of the current state-of-the-art modeling approaches and its performance has been validated by previous studies (Fletcher et al., 1992; Genetti et al., 1999; Genetti, 1999; Grant et al., 1989; Wan et al., 2015; Wang et al., 2015). However, the relative error of this calibrated SFOM model to the original CPD model in PCC-LES is still unclear, since the heating rate of different coal particles in a PCC-LES field can be different due to the effects of turbulence and different particle sizes. The conventional SFOM pyrolysis model is calibrated based on the averaged particle heating rate, and cannot dynamically adjust the pyrolysis reaction according to different local heating rates during the simulation. Hence, it would be necessary to incorporate the CPD model directly and online into the LES framework to improve the accuracy of PCC-LES.

Based on the above motivations, the objectives of this study are: (1) to accurately predict pulverized-coal pyrolysis in a hot turbulent jet using large-eddy simulation that directly incorporates the CPD model; (2) to investigate whether the CPD-coupled LES approach is able to better predict coal particle pyrolysis in a turbulent flow; (3) to study the effects of key parameters,

including the particle diameter, coal type, coal-feeding rate, carrier-phase velocity, and pyrolysis temperature, on pulverized-coal pyrolysis.

Unlike previous PCC-LES studies where the CPD model was separate from LES and therefore an iteration procedure was needed for the CPD to provide appropriate overall chemical kinetic parameters for the conventional SFOM pyrolysis model, in the present study the CPD model has been incorporated into LES in real time. Therefore the pyrolysis modeling of pulverized-coal particles is expected to be more accurate. The online-CPD-coupled LES approach is also used to provide deterministic kinetic parameters for the conventional SFOM pyrolysis model, and a comparison is performed between the two approaches to show the benefit of the developed CPD-coupled LES. Finally, it should be stressed that the focus of the present study is on the pyrolysis stage. The second and third stages of pulverized-coal combustion, i.e., volatile and char combustion, are not considered here. This research strategy offers us an opportunity to achieve a better understanding of pulverized-coal pyrolysis (the first stage of PCC) under different conditions that are directly related to realistic operating conditions of industrial coal-fired furnaces.

Pyrolysis models

The chemistry of pyrolysis is a complex thermal decomposition of raw coal, and related to the breaking of labile bridges between the aromatic structures in the coal. In the pyrolysis process, coal will release light volatile gases and heavier tars (large hydrocarbons), and the residual solid will form char. To describe the pyrolysis of coal particles in LES, two pyrolysis models, i.e., the CPD model and the conventional SFOM pyrolysis model, are employed and their details are presented in the following sections.

Chemical percolation devolatilization (CPD) model

The CPD model (Fletcher et al., 1992; Grant et al., 1989) describes the coal pyrolysis characteristics by using the unique chemical structure of different coals. Under heating in the pyrolysis process, the physical and chemical transformation of coal structure is evaluated based on the number of broken bridges and detached clusters, which is predicted using the percolation statistics for three-dimensional Bethe lattices. The CPD model requires five chemical structural parameters to represent a specific type of coal: the molecular weight of the cluster (MW_{cl}), the molecular weight of side chains (MW_{δ}), the initial fraction of intact bridges (p_0), the coordination number ($\sigma + 1$), and the initial fraction of char bridges (c_0). These parameters can be determined directly from the ^{13}C Nuclear Magnetic Resonance (NMR) analysis, except that the last one c_0 is empirically determined. The performance of the CPD model on predicting the pyrolysis rate and volatile yield compositions has been validated over a wide range of heating rates, temperatures and

coal ranks (Fletcher et al., 1992; Genetti et al., 1999; Genetti, 1999; Grant et al., 1989). In our first-stage work (Wan et al., 2015; Wang et al., 2015), the CPD model has also been systematically validated for pyrolysis of a single coal particle on the time history of the residual mass of the coal particle and the temperature at the particle center.

In the present work, three different coals, i.e., a brown Yallourn coal (YL), a bituminous Vicary Creek coal (VC) and an anthracite Hongay coal (HG), are employed to investigate the pyrolysis characteristics of pulverized-coal particles under various conditions. The proximate and ultimate analysis of the three coals is listed in Table 1. A nonlinear modified quadratic correlation of ^{13}C NMR measurements (Genetti et al., 1999) was employed to estimate the five chemical structural parameters of the coals (Table 2), which are required by the CPD model.

The CPD model was originally developed to predict the volatile yields with time. It has been incorporated into the LES framework in the following way. The CPD status variables that represent the particle pyrolysis status in the original CPD model are recorded and updated for each particle at every time step. In total the CPD status variables have 16 variables and some of the variables are data arrays. These variables represent the progress of the kinetic reactions during coal pyrolysis, e.g., labile dissociation (activating and breaking of bridges), tar/gas release, cross-linking (parts of tar precursors are cross-linked back into the char matrix), in the CPD model.

As shown in Fig. 1, once the particle temperature T_p at time $t + dt$ is obtained, the CPD status

variables at time t for this particle will be restored into the CPD model. Then the CPD model can predict the total volatile yields m_v of the particle at time $t + dt$ according to the instantaneous heating rate of the particle determined by dT_p/dt . Since the recorded CPD status variables include the previous total volatile yields at time t , the volatile release of the particle in the present time step dt can then be obtained. Finally, the mass and species source terms (dm_v/dt and $dm_{Y,n}/dt$) due to the pyrolysis of the particle can be calculated and the CPD status variables of the particle will be updated with the new values at time $t + dt$. The same procedure will be used for all pulverized-coal particles in the computational domain.

As a simplification, the volatile species are assumed to be released at a constant mass ratio during pyrolysis. In the present study, the light gases of the volatile comprise H_2O , CO_2 , CH_4 , CO , C_2H_2 and H_2 , and tar has a formula of $C_{16}H_{24}$ (Devanathan and Saxena, 1987). The compositions of these species can be estimated by the CPD model prior to the LES, using a correlation based on experimental measurements of different coals (Genetti, 1999). It should be mentioned that the compositions predicted by the CPD model have been slightly adjusted to fulfill the elemental balance (elemental mass conservation) (Vascellari et al., 2013a), which is the first principle to comply with. Besides, the maximum volatile yield needs to be determined before the LES, which would in general require an iterative procedure (Rabacal et al., 2015; Stein et al., 2013; Vascellari et al., 2013b), since it can be affected by the heating rate of coal. However, compared with the

iterative procedure when the CPD model is used to calibrate the SFOM model in an LES solver and thus coupled with LES in an offline way, only one iteration will be needed here, because the CPD model has been directly coupled into the LES solver and the maximum yield of volatile is not as sensitive as the pyrolysis kinetics to the heating rate of coal.

Conventional SFOM pyrolysis model

For numerical simulation of pulverized-coal combustion, the classical single first-order reaction model (SFOM) (Badzioch and Hawksley, 1970) has been popularly adopted to model the pyrolysis of a pulverized-coal particle:

$$\frac{dm_v}{dt} = K_v(m_v^* - m_v) \quad , \quad (1)$$

$$K_v = A_v \exp\left(-\frac{E_v}{RT_p}\right) \quad , \quad (2)$$

$$m_v^* = Qm_v^{\prime} \quad . \quad (3)$$

The nomenclature table provides a complete list of the symbols and subscripts. The Q -factor in Eq. (3) accounts for the increase of volatile yields caused by a higher heating rate than in the proximate analysis (Hashimoto et al., 2012).

Since the kinetic parameters in the conventional pyrolysis model are not general, differing from the CPD model, this model is only valid in the range of the conditions and coals on which it is calibrated (Vascellari et al., 2013a). In this work, the numerical results of the online-CPD-coupled LES are employed to calibrate the parameters, i.e., A_v , E_v and Q , of the SFOM model. When the conventional SFOM pyrolysis model is employed in LES, the volatile matter is modeled as a postulated species $C_\alpha H_\beta O_\gamma$ (Franchetti et al., 2013).

Large-eddy simulation

The governing equations for the gas and coal-particle phases are solved in the Eulerian and Lagrangian frameworks, respectively (Xia et al., 2008, 2011, 2013; Yi, 2012). Two-way interactions between the two phases are considered. Pulverized-coal particles are modeled as point sources, since they are small compared to the grid spacing.

Gas phase modeling

The three-dimensional, filtered Navier-Stokes (NS) equations in the low-Mach-number form for mass, momentum, species and temperature are solved for the gas phase and can be written as follows:

$$\frac{\partial^-}{\partial t} + \frac{\partial^- \tilde{u}_j}{\partial x_j} = \bar{S}_{m,p}^-, \quad (4)$$

$$\frac{\partial \bar{u}_i}{\partial t} + \frac{\partial \bar{u}_i \tilde{u}_j}{\partial x_j} = -\frac{\partial \bar{p}}{\partial x_i} + \frac{\partial}{\partial x_j} \left(\bar{u}_{ij} - q_{sgs,mom,ij} \right) + \bar{S}_{mom,p,i} \quad (5)$$

$$\frac{\partial \bar{Y}_n}{\partial t} + \frac{\partial \bar{u}_j \tilde{Y}_n}{\partial x_j} = \frac{\partial}{\partial x_j} \left(-\bar{D}_{diff} \frac{\partial \tilde{Y}_n}{\partial x_j} - q_{sgs,Y,n,j} \right) + \bar{S}_{Y,n} + \bar{S}_{Y,p,n} \quad (6)$$

$$\frac{\partial \bar{T}}{\partial t} + \frac{\partial \bar{u}_j \tilde{T}}{\partial x_j} = \frac{\partial}{\partial x_j} \left(-\bar{D}_{diff} \frac{\partial \tilde{T}}{\partial x_j} - q_{sgs,T,j} \right) + \bar{S}_T + \bar{S}_{T,p} + \bar{S}_{T,R} \quad (7)$$

These equations have been simplified based on the following assumptions: the thermodynamic pressure is constant; the body forces are zero; the viscous heating is negligible; the specific heat capacities of all the gas species are equal and constant ($C_{p,g} = 1200 \text{ J}/(\text{kg} \cdot \text{K})$). Since nitrogen is the major species of the gas mixture, we have chosen a typical value of the heat capacity, $1200 \text{ J}/(\text{kg} \cdot \text{K})$, of nitrogen between the lowest (300 K) and highest (2000 K) temperature in the present study as the heat capacity of the gas mixture as a simplification to save computational cost. The influence of the constant $C_{p,g}$ assumption on the results has been investigated by comparing LES results between two cases which use a $C_{p,g}$ varying with temperature and species mass fractions and a constant $C_{p,g} = 1200 \text{ J}/(\text{kg} \cdot \text{K})$, respectively. It has been found that the results of the variable- $C_{p,g}$ case and the constant- $C_{p,g}$ case are very similar. For instance, the difference of the mass fractions of tar and gas phase temperature along the centerline between the two cases is found to be less than 10% (not shown). Therefore using the constant gas-phase heat capacity is acceptable for the present study.

The subgrid-scale (SGS) terms, $q_{sgs,mom,ij}$, $q_{sgs,Y,n,j}$ and $q_{sgs,T,j}$, are calculated by the Germano dynamic model (Germano et al., 1991; Lilly, 1992; Moin et al., 1991). The source terms due to pulverized-coal particles, $\bar{S}_{m,p}$, $\bar{S}_{mom,p,i}$, $\bar{S}_{Y,p,n}$ and $\bar{S}_{T,p}$, are calculated using the particle-source-in-cell (PSI-CELL) model (Crowe et al., 1977). $\bar{S}_{Y,n}$ and \bar{S}_T are the chemical reaction source terms. $\bar{S}_{T,R}$ is the source term due to radiative heat transfer. The viscous stress tensor in the momentum equation is

$$\tau_{ij} = -\left(\frac{\partial \tilde{u}_i}{\partial x_j} + \frac{\partial \tilde{u}_j}{\partial x_i}\right) - \frac{2}{3} \frac{\partial \tilde{u}_k}{\partial x_k} \delta_{ij} \quad (8)$$

The molecular viscosity μ is determined using the Sutherland's Law (Sutherland, 1893) of N_2 , considering N_2 is the major species of the gas mixture. Based on the assumptions of a constant Lewis number ($Le = 1.0$) and Prandtl number ($Pr = 0.7$) (Xia et al., 2011), the molecular thermal and mass diffusivity coefficients are calculated by $\lambda = \mu / (Pr \cdot \rho)$ and $\bar{D}_{diff} = \mu / Le$, respectively.

Particle phase modeling

The Lagrangian equations tracing the transient position, velocity, temperature and mass of each particle can be written as:

$$\frac{dx_{p,j}}{dt} = u_{p,j} \quad (9)$$

$$\frac{du_{p,j}}{dt} = \frac{f}{p} (\tilde{u}_j - u_{p,j}) + W_{sgs,j} , \quad (10)$$

$$\frac{dT_p}{dt} = \frac{(Q_{conv} + Q_{rad} + Q_{dev})}{m_p C_{p,p}} , \quad (11)$$

$$\frac{dm_p}{dt} = -\frac{dm_v}{dt} . \quad (12)$$

In Eq. (10), the dynamic response time of a particle is $\tau_p = \rho_p d_p^2 / (18\mu)$. The drag coefficient f is empirically modeled by, considering the high particle Reynolds number effects and the blowing effects due to volatiles at the surface of a pulverized-coal particle (Miller and Bellan, 1999):

$$f = \frac{1 + 0.0545 \text{Re}_{sl} + 0.1 \text{Re}_{sl}^{1/2} (1 - 0.03 \text{Re}_{sl})}{1 + a |\text{Re}_b|^b} , \quad (13)$$

where the model parameters are

$$a = 0.09 + 0.077 \exp(-0.4 \text{Re}_{sl}) \quad \text{and} \quad b = 0.4 + 0.77 \exp(-0.04 \text{Re}_{sl}) . \quad (14)$$

The particle Reynolds number is defined as $\text{Re}_{sl} = \rho_p u_{sl} / \mu$, where the magnitude of the slip velocity between the gas and particle phases u_{sl} is $u_{sl} = |\tilde{\mathbf{u}} - \mathbf{u}_p|$. $\text{Re}_b = \rho_p u_b / \mu$ is based on the blowing velocity u_b , which is determined by $u_b = -(dm_p/dt) / (\rho_p d_p)$. The effects of unresolved SGS turbulence on particle acceleration ($W_{sgs,j}$) are estimated using a stochastic Markov model

(Jones et al., 2011), although only minor differences were found between the results of the LESs including or excluding this model.

The convective heat transfer between the gas and particle phases in Eq. (11) is

$$Q_{conv} = \frac{\text{Nu} C_{p,g} m_p}{3 \text{Pr}_p} (\tilde{T} - T_p) , \quad (15)$$

where the Nusselt number is calculated by the Ranz-Marshall correlations (Ranz and Marshall, 1952): $\text{Nu} = 2 + 0.552 \text{Re}_{st}^{1/2} \text{Pr}^{1/3}$. The heat transfer due to radiation is

$$Q_{rad} = \epsilon_p d_p^2 (T_R^4 - T_p^4) , \quad (16)$$

where the radiation temperature is computed by $T_R = (G/4)^{1/4}$, and the incident radiation G is calculated using the Discrete Ordinates Method. The particle emissivity ϵ_p is set to 0.9 (Lu et al., 2010). Finally, the heat transfer due to pyrolysis (devolatilization) is

$$Q_{dev} = \frac{dm_p}{dt} \Delta h_{dev} , \quad (17)$$

with the heat of the pyrolysis reaction set as $\Delta h_{dev} = 418.6 \times 10^3$ J/kg (Genetti, 1999). The specific heat capacity of the coals is determined by (Yi, 2012)

$$C_{p,p} = 836.0 + 1.53 \times (T_p - 273.0) - 5.4 \times 10^{-4} (T_p - 273.0)^2 . \quad (18)$$

Two-way coupling terms

The source terms coupling the particle and gas phases are obtained by integrating the contributions of all particles in the local control volume (the local grid cell):

$$\bar{S}_{m,p} = -\frac{1}{V_{cv}} \sum_{p \in cv} \frac{dm_p}{dt} = \frac{1}{V_{cv}} \sum_{p \in cv} \frac{dm_v}{dt} , \quad (19)$$

$$\bar{S}_{mom,p,i} = -\frac{1}{V_{cv}} \sum_{p \in cv} \frac{dm_p u_{p,i}}{dt} , \quad (20)$$

$$\bar{S}_{T,p} = -\frac{1}{V_{cv} C_{p,g}} \sum_{p \in cv} \left(Q_{conv} + Q_{rad} + C_{p,g} T_p \frac{dm_p}{dt} \right) , \quad (21)$$

$$\bar{S}_{Y,p,n} = \frac{1}{V_{cv}} \sum_{p \in cv} \frac{dm_{Y,n}}{dt} . \quad (22)$$

The volatile release rate dm_v/dt in Eq. (19) and species release rate $dm_{Y,n}/dt$ in Eq. (22) can be determined from the coal pyrolysis model.

Gas phase reaction

The thermal cracking reaction of tar (a secondary pyrolysis reaction) is approximated by



$C_{16}H_{24}$ is used as the formula of tar (Devanathan and Saxena, 1987). Since the chemical time scale of the reaction (23) is much longer than the subgrid turbulence time scale, the subgrid-scale fluctuations can be neglected in the estimation of the filtered reaction rate (Poinsot and Veynante, 2012), which can therefore be determined using the Arrhenius law

$$\bar{\tau} = A_{tar} \frac{\bar{Y}_{tar}}{W_{tar}} \exp\left(-\frac{E_{tar}}{R\bar{T}}\right). \quad (24)$$

The reaction parameters are $A_{tar} = 10^{13} \text{ s}^{-1}$ and $E_{tar} = 272 \text{ kJ/mol}$ (Devanathan and Saxena, 1987). Here, the subgrid turbulence time scale is estimated by $\tau_{sgs} = (\tau_K \tau_\Delta)^{1/2}$ (Berglund et al., 2010). Since reaction (23) is thermal decomposing of the tar, turbulent mixing between fuel and oxidizer is not relevant. In addition, for the present LES, more than 80% of the TKE (turbulence kinetic energy) has been resolved, especially in the jet centerline region. Taking these two factors into consideration, we use $W_{tar} / A_{tar} \exp(-E_{tar} / R\bar{T})$ to estimate the chemical time scale τ_{chem} , according to $\tau_{chem} = \partial\rho Y_{tar} / \partial\omega_{Y,tar}$ (Prüfert et al., 2014). It was found that the ratio τ_{chem} / τ_{sgs} is large in the central region where the tar decomposes (not shown), justifying Eq. (24).

The source terms on the RHS of the species equation (6) and the temperature equation (7) due to the reaction are calculated by, respectively,

$$\bar{\tau}_{Y,n} = \bar{W}_n \bar{\tau} \quad \text{and} \quad \bar{\tau}_T = -\Delta h_{dev} \bar{W}_{tar} \bar{\tau} / C_{p,g}. \quad (25)$$

Radiation modeling

The radiative transfer equation (RTE)

$$\vec{s} \cdot \nabla I(\vec{r}, \vec{s}) + (k + k_p + \rho_p) I(\vec{r}, \vec{s}) = k \frac{\tilde{T}^4}{4} + E_p + \frac{\rho_p}{4} \int_0^4 I(\vec{r}, \vec{s}') \Phi(\vec{s} \cdot \vec{s}') d\Omega' \quad (26)$$

is solved using the Discrete Ordinates Method (DOM) (Chandrasekhar, 1960; Franchetti et al., 2013; Modest, 2013; Rabacal et al., 2015). It is discretized and solved for 24 directions using the S_4 angular discretization scheme (Fiveland, 1988; Franchetti et al., 2013; Modest, 2013; Rabacal et al., 2015; Truelove, 1987). In this study isotropic scattering is applied, which implies the scattering phase function $\Phi(\vec{s} \cdot \vec{s}') = 1$.

With the grey-gas assumption, the gas absorption coefficient is determined by (Rabacal et al., 2015)

$$k = 0.2 \bar{X}_{fuel} + 0.1 (\bar{X}_{CO_2} + \bar{X}_{H_2O}) \quad (27)$$

where the subscript *fuel* denotes CH₄, CO, C₂H₂ and tar. The unit of the constants 0.2 and 0.1 is m⁻¹. The equivalent absorption and scattering coefficients of a pulverized-coal particle in the local control volume are defined by

$$k_p = \frac{\rho_p}{V_{cv}} \sum_{p \in cv} \frac{d_p^2}{4} \quad \text{and} \quad \rho_p = \frac{(1 - \rho_p)}{V_{cv}} \sum_{p \in cv} \frac{d_p^2}{4} \quad (28)$$

respectively. The equivalent emission of the particle is defined by

$$E_p = \frac{\rho_p}{V_{cv}} \sum_{p \in cv} \frac{d_p^2}{4} \frac{T_p^4}{\rho_p} . \quad (29)$$

The radiative transfer equation (Eq. (26)) is iteratively solved until the maximum residual of the radiation intensity $I(\vec{r}, \vec{s})$ drops below a preset error margin (10^{-6}). Then the radiative source term in the energy equation (7) can be calculated by

$$\bar{S}_{T,R} = \frac{1}{C_{p,g}} \left(-4 \left(k \frac{\tilde{T}^4}{\rho_p} + E_p \right) + (k + k_p) G \right) , \quad (30)$$

where $G = \int_0^4 I(\vec{r}, \vec{s}) d\Omega$ is the incident radiation.

Code validation

There is currently no suitable experimental or numerical data available for direct comparison on pulverized-coal pyrolysis in a turbulent flow. To demonstrate the capability of the two-phase LES solver, a validation has been performed on a particle-laden free round jet (Fleckhaus et al., 1987).

A comprehensive validation of the CPD model on predicting coal particle pyrolysis has been performed in previous studies (Fletcher et al., 1992; Genetti et al., 1999; Genetti, 1999; Grant et al., 1989; Wan et al., 2015; Wang et al., 2015).

For the particle-laden turbulent air jet (Fleckhaus et al., 1987), the nozzle diameter (D) was 13 mm, and the air flow rate was 3.747×10^{-3} kg/s. The particles were spherical glass beads with a density of 2590 kg/m^3 . The mass-loading ratio of the particles to the gas carrier phase was 0.3. The mean particle diameter was $64 \text{ }\mu\text{m}$ and the particle size distribution was the same as in Fleckhaus et al. (1987). The large-eddy simulation was run on a 0.75-million-cell mesh. A separate, pre-processed pipe-flow LES with periodic streamwise boundary conditions was used to provide turbulent inflow boundary conditions for the gas phase (Pierce and Moin, 1998; Schlüter et al., 2004). A power-law profile was used for the particle inlet velocity with the exponent set to be $1/27.6$, i.e., $U_{p,r}/U_{p,c} = (1 - 2r/D)^{1/27.6}$ (Fairweather and Hurn, 2008), and the particle velocity ($U_{p,c}$) on the centerline was chosen to be 28.0 m/s to achieve the best agreement with the experimental data at 10 nozzle diameters downstream of the inlet.

The LES results of the particle-laden turbulent jet are compared with the experimental data (Fleckhaus et al., 1987) and RANS results (Fairweather and Hurn, 2008) in Fig. 2. The LES predictions of the mean axial velocity, TKE (turbulence kinetic energy) and shear stress of the gas phase show a very good agreement with the RANS results using the Reynolds-stress and $k-\epsilon$ models. Compared to the experimental data, both the LES and RANS can give a reasonable prediction on the gas phase statistics, although they both tend to over-predict the TKE and shear stress at $10 D$ and $20 D$ downstream. For the particle phase, the mean axial velocity prediction of

the LES agrees well with the experimental and RANS data. Both the LES and RANS over-predict the particle TKE, especially the centerline results at $x/D = 30$. However, the LES predicts much better the particle shear stress than the RANS does. Overall, the prediction of the LES code on the particle-laden turbulent jet is acceptably good as compared to previous experimental and numerical data.

Computational setup and numerical schemes

The size of the three-dimensional computational domain is 0.78 m ($60 D$) in length and 0.3 m ($23 D$) in width. The domain is decomposed into 1.56 million grid cells with more than 90% of the cells are located in the physical statistics zone (Fig. 3). The surrounding unphysical buffer zone is used to alleviate the effects of numerical boundary conditions and improve numerical stability. The minimum grid spacing is 0.2 mm ($0.015 D$) at the edge of the nozzle, and the maximum one in the statistics zone is 9.6 mm ($0.74 D$) at the downstream exit of the domain. The smallest and largest cell volumes are 0.1 mm^3 and 711.8 mm^3 , respectively. The highest particle volume fraction of the baseline case A (see Table 3) is 3.4% in the whole domain, while in most of the grid cells the particle volume fraction is much lower. The grid sensitivity has been checked using a fine grid of 3.8 million cells with the minimum and maximal grid spacing of 0.16 mm and 7.4 mm, respectively. The difference of the simulation results between the coarse- and fine-grid LES is less

than 15% for major flow quantities such as gas-phase temperature and volatile species mass fractions along the centerline, where most of the coal particles locate.

In order to investigate the effect of the particle diameter, coal type, coal-feeding rate, carrier-phase velocity, and pyrolysis temperature on pulverized-coal pyrolysis characteristics in a hot turbulent jet, parametric studies have been conducted (Table 3).

For the baseline case, the primary nozzle inlet is located at the center of $x = 0$ face, with a nozzle diameter (D) of 13 mm. Nitrogen gas (bulk velocity: 10 m/s, 300 K) carrying pulverized-coal particles (mass flow rate: 5.1×10^{-4} kg/s, 300 K) are injected through the nozzle. The inflow boundary condition for the gas phase of the primary pulverized-coal jet is provided by a separate pipe-flow LES (Pierce and Moin, 1998; Schlüter et al., 2004). The Reynolds number of the primary jet is 8200. A log-normal distribution ($d_{p,min} = 10 \mu\text{m}$, $d_{p,max} = 100 \mu\text{m}$, $d_{p,mean} = 45 \mu\text{m}$, $d_{p,sd} = 120 \mu\text{m}$) is used to model the particle diameter distribution. A particle's location at the nozzle inlet is determined with a random uniform distribution over the primary inlet face, and the velocity of a particle is assumed to be the same as the gas velocity at the particle location. The coal particle density is set to be 1400 kg/m^3 . A hot nitrogen co-flow (bulk velocity: 0.2 m/s, 2000 K) surrounds the primary inlet to provide a high-temperature ambient to enable pulverized-coal pyrolysis. Convective and zero-gradient boundary conditions are applied at the exit and side of the domain, respectively. The CPD model is employed to describe the pyrolysis process of each coal

particle. During the pyrolysis, the particle diameter is assumed to be constant, while the particle density decreases according to the mass loss due to the release of volatiles.

For all the other cases in Table 3, the computational setup is identical to the baseline case A, except that one parameter has been varied in each case to investigate the effects of important operating parameters on pulverized-coal pyrolysis characteristics.

For the numerical schemes, the second-order Crank-Nicolson scheme is used for time advancement. A third-order weighted essentially non-oscillatory (WENO) scheme (Liu et al., 1994) is used for the discretization of the scalar advection terms in the species and temperature equations, while a second-order central-difference scheme is employed for the scalar diffusion terms in the species and temperature equations and all terms in the momentum equation (Mittal and Pitsch, 2013). A staggered grid is used, where velocity components are stored at the cell faces, whereas the other scalars are stored at the cell centers. A characteristic flow-through time for the statistics zone can be estimated as $60 D / (0.5 U_{bulk}) = 0.156$ s. It takes 5-6 flow-through times to stabilize the gas-solid two-phase jet, and another 3-4 flow-through times to obtain the statistics. One typical case running 10 flow-through times requires approximately 11,520 core hours, and the most computationally expensive case (B1) requires approximately 41,600 core hours. It should be noted that each physical particle is tracked in the present LES study, and the CPD model is applied

on each of them during the simulation. In total there are 0.65 million particles in the computational domain for the baseline case A and 6.2 million for Case B1.

Results and discussion

Instantaneous two-phase flow fields

After injected with the nitrogen flow, a coal particle is gradually heated up and its density decreases due to pyrolysis. As the particle diameter is assumed to be constant during the pyrolysis, the decrease of the particle density designates the release of volatiles. An instantaneous snapshot of pulverized-coal pyrolysis in the hot turbulent nitrogen jet in Case A is shown in Fig. 4. The iso-surface of $Y_{CH_4} = 0.25\%$ is colored by the gas temperature. 0.1% of the total particles are plotted. Each particle is colored by its density and the size of each particle illustrates its diameter.

To better explain the pulverized-coal pyrolysis characteristics in a high-temperature turbulent flow, three pyrolysis regions are defined. The first one is a preheating region, where only some isolated volatile zones (IVZs) can be observed. In this region, pulverized-coal particles carried by the cold primary nitrogen jet are heated by the hot co-flow through turbulent mixing and radiation. The temperature of some particles with relatively small diameters on the jet periphery becomes higher than the lower limit temperature of pyrolysis and volatiles start to be generated. The second pyrolysis region is a growing volatile (GV) region, where more and more coal particles start

pyrolysis and the volatile zone is growing. The third pyrolysis region is a continuous volatile (CV) region, where the pulverized-coal pyrolysis achieves a stable state and the volatile iso-surfaces become a continuous large surface, as illustrated by the $Y_{CH_4} = 0.25\%$ iso-surface in Fig. 4. These three regions have also been found in previous pulverized-coal combustion studies (Yamamoto et al., 2011), where the gas temperature was employed as the characteristic variable to identify three combustion regions instead of the volatile mass fraction in the present study. The similarity of the three regions between the present study and the previous pulverized-coal combustion study (Yamamoto et al., 2011) corroborates that the pyrolysis stage has a significant influence on the pulverized-coal combustion process.

In the enlarged view of the GV region (see Fig. 4), the dynamic pyrolysis process of pulverized-coal particles has been clearly presented. It can be found that the particles located inside the $Y_{CH_4} = 0.25\%$ iso-surface are mainly raw particles, while the particles located outside the iso-surface are pyrolyzed with a lower density. When a coal particle moves from the low-temperature primary jet to the high-temperature co-flow, pyrolysis occurs and volatile is generated from the coal particle.

Comparison between predictions of LES using an online CPD model and a conventional pyrolysis model (SFOM)

To clarify the influence of an online CPD model on the predictions of coal pyrolysis in turbulent flow, Case AA has been setup with the same parameters as in Case A except that the SFOM model is employed for pyrolysis modeling. Since the kinetic parameters in the SFOM model are not general, this model is only valid in the range of operating conditions and coals on which it is calibrated (Vascellari et al., 2013a).

In this work, the averaged statistics of the coal particle temperature and axial velocity (for estimating the resident time of a particle) on the centerline of the online-CPD-coupled LES (Case A) were employed to calibrate the kinetic parameters of the SFOM model for Case AA. With the correlation between the particle temperature and its resident time, a standalone CPD model was used to predict the pyrolysis process of a single coal particle to generate the profile of the mass loss of the coal particle with time. Then this profile was fitted by the conventional SFOM pyrolysis model to obtain the calibrated kinetic parameters. The instantaneous coal particle heating rate in this calibration process was found to have a magnitude of 10^4 - 10^5 K/s. The obtained kinetic parameters are A_v ($1.0 \times 10^4 \text{ s}^{-1}$), E_v ($4.11 \times 10^4 \text{ J/mol}$) and Q (1.12).

The predictions of the LESs using the online CPD and conventional pyrolysis models are compared in this subsection. To facilitate the description, “CPD-LES” and “Conventional-LES” have been used to designate the two LES cases, i.e., Cases A and AA in Table 3.

The CPD-LES and Conventional-LES produced similar gas- and particle-phase statistics (not shown here), which indicates that using the particle statistics on the centerline to calibrate the kinetic parameters of the SFOM is an optimal choice since most of the pulverized-coal particles locate around the centerline for the case under investigation. It should be noted, however, that such a profile of particle statistics would not be available in general.

Although comparisons on averaged gas- and particle-phase statistics are acceptably good, important discrepancy has been identified in instantaneous particle pyrolysis status, as shown below. The better prediction given by the CPD-LES is crucially important for high-fidelity simulation of pulverized-coal combustion, especially as tracing harmful minor species of alkali metal is the key objective of our next-stage research.

In Fig. 5, the scatter plots of the residual mass of a pulverized-coal particle in the computational domain vs. the particle temperature, denoting the instantaneous particle pyrolysis state, have been shown in Fig. 5a-d for the CPD-LES and in Fig. 5e-h for the Conventional-LES, respectively. All the particles have been grouped in 4 classes according to their sizes, i.e., 10-30 μm , 30-50 μm , 50-75 μm and 75-100 μm . The red line denotes the pyrolysis profile of a single coal particle predicted by the standalone CPD model in the abovementioned calibration process, which has been used as a characteristic pyrolysis profile to calibrate the conventional SFOM pyrolysis model used in the Conventional-LES. It can be found that the pyrolysis characteristics of pulverized-coal

particles in the hot turbulent jet mainly follow that of a single coal particle predicted by the standalone CPD model (Fig. 5a-d) as shown by the red line, which also indicates that the pyrolysis profile of a single coal particle indeed represents the overall pyrolysis characteristics of coal particles in the CPD-LES well. As shown in Fig. 5e-h, the instantaneous particle pyrolysis state predicted by the Conventional-LES also largely follows the red line. However, fluctuations can be observed around the red line in both the CPD-LES and Conventional-LES, and smaller particles tend to have larger deviations from the red line.

Figure 6 is the scatter plots of the instantaneous particle pyrolysis state of all the particles in the CPD-LES (Fig. 6a) and Conventional-LES (Fig. 6b). To facilitate comparison and discussion, the pyrolysis profiles of a single coal particle under different heating rates (NOT in turbulent flow) predicted by the standalone CPD model (Fig. 6a) and the calibrated SFOM model (Fig. 6b) are also shown. In Fig. 6a, the fluctuations of the data samples can be observed in Regions I and II. In Region II, the small fluctuation can be attributed to flow turbulence effects and different heating rates of different particles. As shown by the pyrolysis profiles of a single coal particle, when the heating rate of the particle increases, its pyrolysis profile moves towards the right side of the figure. In Region I, Fig. 6a indicates that for a particle with the same residual mass, its temperature is much lower than the temperature of coal particles in Region II. Therefore, this particle has been transported to a low-temperature area (e.g. the primary jet core) from a high-temperature area (e.g.

the jet periphery) due to turbulent convection and/or diffusion, and its pyrolysis is suspended. Figure 5 shows that these fluctuations are mainly due to small particles (diameter < 50 μm). The Conventional-LES (Fig. 6b) shows similar fluctuations in the Regions I and II to those in the CPD-LES.

On the other hand, the Conventional-LES results show a large scatter in Region III (Fig. 6b), which is, however, not shown in Fig. 5a-d and Fig. 6a predicted by the CPD-LES. Particles in Region III are experiencing a high heating rate. Comparing the 4 pyrolysis profiles of a single coal particle under different heating rates predicted by the CPD model (Fig. 6a) and the calibrated SFOM model (Fig. 6b), it can be concluded that the SFOM model can give a reasonable prediction when the heating rate is at a magnitude of 10^4 K/s, which is on the same order of magnitude of the heating rate found in the calibration process. When the heating rate is higher (10^5 - 10^6 K/s), the SFOM model significantly under-predicts the pyrolysis rate and therefore its pyrolysis profile moves largely and incorrectly toward the right side of the figure in contrast with the corresponding pyrolysis profile predicted by the CPD model. The data points in Region III of the Conventional-LES (Fig. 6b) are caused by this under-prediction of the pyrolysis rate of the SFOM model for the particles experiencing a higher heating rate than that on which the SFOM model is calibrated. As a further proof for this statement, Fig. 7 shows the scatter plots of the normalized instantaneous particle pyrolysis rate vs. particle temperature for the particles experiencing a high

heating rate ($> 10^5$ K/s) in the CPD-LES and Conventional-LES. The particles in the CPD-LES (Fig. 7a) achieve a higher pyrolysis rate, which is under-predicted by the Conventional-LES (Fig. 7b). It indicates that these particles are more reactive in pyrolysis in the CPD-LES and the calibrated SFOM model used in the Conventional-LES cannot properly model the pyrolysis characteristics of these particles.

Therefore Region III in Fig. 6b is an unphysical zone due to under-prediction of the SFOM on the pyrolysis rate of a coal particle at a higher heating rate than the one for calibration. From Figs. 5a-d and 6a, it is clear that for the CPD-LES there is no scatter towards Region III, demonstrating that the online CPD model can adjust the particle pyrolysis state according to the local heating rate. However, the kinetic parameters (A_v , E_v and Q) in the conventional pyrolysis model are calibrated and preset, and therefore the Conventional-LES cannot adjust the pyrolysis kinetics of a coal particle according to its local heating rate, leading to the unphysical large scatter in Region III in Figs. 5e-h and 6b.

The computational cost of the Conventional-LES and CPD-LES are compared in Table 4. Compared to the Conventional-LES, the CPD-LES costs 51.4% more computational time on average for one time step. For the particle equations, the computational cost is increased by 121.4%. The detailed pyrolysis model (CPD model) in the CPD-LES is responsible for the increase of the computational cost on the particle transport equations. In addition, a significant

increase of computational cost (286.8%) is found on scalar transport equations. This is because the volatile comprises 7 species in the CPD-LES; while in the Conventional-LES the volatile is modeled as one postulated species $C_\alpha H_\beta O_\gamma$. Although the CPD-LES costs more computation time per time step, it should be noted that the CPD-LES only requires one iteration to obtain the maximum volatile yield as an input parameter for the CPD-coupled LES solver. Therefore two LESs will be needed in total; while the Conventional-LES will require three complete LESs (Rabacal et al., 2015) to get the calibrated kinetic parameters when the results of the CPD-LES is unavailable, which is a general situation. After taking the iteration procedure into consideration, the computational cost of the two LES methods is similar with the setup in the present work.

Overall, the performance of the CPD-LES method is found to be better than the calibrated Conventional-LES method. The SFOM pyrolysis model in the Conventional-LES approach cannot adjust its pyrolysis kinetic parameters according to the real-time heating rate of different particles. In the instantaneous scatter plots of the pyrolysis characteristics of coal particles shown in Figs. 5-7, the weakness of the conventional SFOM pyrolysis model, although calibrated by the results of CPD-LES (which would not be available in general for an LES solver using the SFOM), has been clearly demonstrated.

Parametric study on pulverized-coal pyrolysis in a hot turbulent jet

In total 9 cases (see Table 3) were performed to investigate the effects of important operating parameters, i.e., the particle diameter (Case B1/B2), coal type (Case C1/C2), coal-feeding rate (Case D1/D2), carrier-phase velocity (Case E) and pyrolysis temperature (Case F), on pulverized-coal pyrolysis characteristics using the developed CPD-LES method. To better present and compare the instantaneous volatile fields of different cases, the local stoichiometric ratio of the gas phase (SR_g) (Yamamoto et al., 2011) is introduced as a quantified measure of the local total amount of the seven volatile species (H_2O , CO_2 , CH_4 , CO , C_2H_2 , H_2 and tar) predicted by CPD-LES. In a combustion case, SR_g is defined as

$$SR_g = (\text{actual oxygen mass}) / (\text{oxygen mass that is required for complete combustion}).$$

It is easy to see that SR_g is the inverse of the local equivalence ratio ϕ , i.e., $SR_g = 1 / \phi$. In the present pulverized-coal pyrolysis study, since there is no oxygen in the gas phase, we approximate SR_g by

$$SR_g = (\text{nitrogen mass} \times 0.233) / (\text{oxygen mass that is required for complete combustion}).$$

The local SR_g was considered to be one of the most important quantitative measures to predict the ignition in PCC. In PCC, as coal particles are heated and then yield volatiles, the gaseous volatile fuels are locally ignited where the ignition condition is met. It was found that $SR_g = 1.24$ can be used to predict the ignition location in previous PCC-LES studies (Yamamoto et al., 2011) and is

also used here as an estimate of the lift-off height of ignition in a PCC case under identical operating conditions. Since $SR_g = 5.0$ indicates that the local gaseous mixture is very lean, the downstream location where this iso-surface starts to appear is used as a quantified estimate for where volatile starts to be generated, i.e., the isolated volatile zone starts to appear. In addition, the $SR_g = 5.0$ iso-surface can be seen as an outmost surface enclosing all the volatiles produced in the pyrolysis process. The iso-surfaces of $SR_g = 1.24$ and $SR_g = 5.0$ predicted by CPD-LES are shown in Fig. 8 for all the cases defined in Table 3.

In the present study, two pyrolysis lift-off heights (PLHs) are defined by the distances from the nozzle to the downstream location where the iso-surfaces of the above two SR_g 's (see the illustration in Case A in Fig. 8) start to form. The PLHs of different cases is compared in Fig. 9. Finally, the instantaneous pyrolysis rate of each pulverized-coal particle is shown in Fig. 10 for all the cases, and Fig. 11 shows the mean pyrolysis rate of all pulverized-coal particles for which the pyrolysis rate is not zero in the computational domain.

Effects of the particle diameter

Case A is used as a baseline for the comparison. From Cases B1/B2, the effect of the particle diameter on the pyrolysis characteristics is demonstrated. When smaller coal particles are employed in Case B1, pyrolysis occurs earlier (Fig. 10) and the isolated volatile zone appears

closer to the nozzle (Fig. 8). It can be observed that the fine particles at the jet periphery in Case B1 achieve a high pyrolysis rate in the region of $x < 10D$ (Fig. 10). While the particle diameter becomes larger in Case B2, the pyrolysis occurs later (Fig. 10) and the isolated volatile zone moves away from the nozzle (Fig. 8). Since coal particles are heated through convective and radiative heat transfer and the ratio of the surface area to mass of a smaller particle is larger compared to that of a larger particle, the temperature of a smaller particle will rise more rapidly when subjected to convective and radiative heating. The particle temperature largely determines the rate of loss of the particle mass. In addition, smaller particles are easier to be transported to the hot jet periphery. Comparing Case B1 and Case B2 in Fig. 10, it is clear that the fine particles in Case B1 tend to disperse away from the centerline while the large particles in Case B2 tend to stay within the jet core area. Hence, finer pulverized-coal particles are easier to be pyrolyzed in a hot turbulent flow. From Fig. 9, it can be found that a larger mean particle diameter leads to the increase of the PLHs. To quantify the effects of the particle diameter on pulverized-coal pyrolysis, the mean pyrolysis rate of all reacting particles in the computational domain are shown in Fig. 11. Comparing Cases A, B1 and B2, it can be found that enhancement of pyrolysis is more significant when the mean particle diameter decreases from 45 μm (Case A) to 22.5 μm (Case B1) than from 90 μm (Case B1) to 45 μm (Case A).

Effects of the coal type

Comparing Cases C1/C2 with Case A, it can be found that the pyrolysis characteristics of different types of coal are distinctively different (Figs. 8-11). Since the brown Yallourn coal (Case C1) contains more volatiles (see Table 1), the highest volatile yield rate is achieved in Case C1 (Figs. 10 and 11) as compared to Cases A and C2, and the isolated volatile zone appears closer to the nozzle in Case C1 (Figs. 8 and 9). For the anthracite Hongay coal (Case C2), few volatiles have been produced due to its very low volatile content (see Table 1). Based on the comparison, it is easy to conclude that the anthracite is much more difficult to be ignited and burned in PCC furnaces than the brown Yallourn (Case C1) and bituminous Vicary Creek (Case A) coals. This is due to the fact that after the first-stage pyrolysis, the second-stage gas-phase volatile combustion will take the dominant role in PCC compared to the third-stage solid-phase char combustion. In Case C2, the PLH for $SR_g = 1.24$ is unavailable (Fig. 9) because the volatile concentration is too low. It indicates the pulverized-coal-particle-laden jet cannot be ignited under this condition.

Effects of the coal-feeding rate

For Cases D1/D2, Fig. 8 shows that when the coal-feeding rate is higher, more volatiles will be produced. A high concentration of volatiles benefits the ignition. In addition, the PLHs become smaller when the coal-feeding rate rises (Fig. 9). On the other hand, when we look into the pyrolysis characteristics of each particle (Fig. 10), it can be found that the magnitudes of the pyrolysis rate between Cases A and D1/D2 are similar, but more particles are pyrolyzed in Case

D1. The comparison of the mean pyrolysis rate between Cases A and D1/D2 (Fig. 11) also suggests that the effects of the coal-feeding rate on the pyrolysis rate of pulverized-coal particles are minor. Therefore, the high concentration of volatiles in Case D1 is mainly because more coal particles are injected and pyrolyzed.

Effects of the carrier-phase velocity

From the comparison between Case A and Case E, it can be seen that the release of volatile is delayed (Fig. 10) and the volatile mass fractions become lower (Fig. 8) as the carrier-phase velocity increases. The volatile zone moves away from the nozzle and therefore the PLHs become larger (Fig. 9). Comparing Case E with Case D2, the sizes of the volatile zone illustrated by the $SR_g = 5.0$ iso-surface in the two cases are very similar. The reason lies in that the inlet stoichiometric ratio (SR_{in}) is the same for the two cases ($= 1/6$), where the SR_{in} is defined as

$SR_{in} = (\text{the inlet nitrogen mass} \times 0.233) / (\text{oxygen mass that is required for completely burning the coal at the inlet}).$

The comparison of Case E with Case A on the PLHs (Fig. 9) and volatile zones (Fig. 8) suggests that a higher carrier-phase velocity has a disadvantageous effect on pyrolysis. However, the pyrolysis rate of each particle (Fig. 10) and the mean pyrolysis rate (Fig. 11) show that the

pyrolysis is actually enhanced with a higher carrier-phase velocity due to the higher Reynolds number and stronger turbulent mixing.

Effects of the pyrolysis temperature

Finally, the effects of the pyrolysis temperature is shown by the comparison between Cases F and A. Obviously, the pyrolysis process becomes slower (Fig. 10) and the total volatile zone smaller (Fig. 8) when the ambient temperature decreases. As the heating of coal particles takes a longer time in Case F, the pyrolysis rate decreases (Fig. 11) and the PLHs become larger than that in Case A (Fig. 9). In a PCC case, the pyrolysis stage (the first stage of PCC) and volatile combustion stage (the second stage) will interact with each other. When the temperature becomes higher, the pyrolysis of pulverized-coal particles will be enhanced and more volatiles released. The higher volatile concentration will then lead to stronger volatile combustion and therefore enhance the pyrolysis process in turn.

Conclusions

An LES solver directly incorporating an advanced pyrolysis model CPD has been developed and employed to investigate pulverized-coal pyrolysis characteristics in a hot turbulent jet. The simulation results of the developed online-CPD-coupled LES approach were used to calibrate the kinetic parameters of the conventional pyrolysis model SFOM. The results of the CPD-LES and

SFOM-LES are then compared. The performance of the online-CPD-coupled LES method was found to be better than the LES method incorporating the calibrated SFOM. The conventional pyrolysis model SFOM, although calibrated by the results of the online-CPD-coupled LES, could not adjust its kinetic parameters according to the local heating rate of different particles, and therefore it cannot fully reproduce the instantaneous pyrolysis characteristics of pulverized-coal particles.

The effects of different parameters, including the particle diameter, coal type, coal-feeding rate, carrier-phase velocity, and pyrolysis temperature, on the pulverized-coal pyrolysis in a hot turbulent jet flow were investigated through parametric studies using the online-CPD-coupled LES method. Through the analysis of both instantaneous volatile fields and the particle pyrolysis rate, it was found that a smaller mean diameter of pulverized-coal particles, coal with a higher volatile content, a higher coal-feeding rate or a higher pyrolysis temperature will facilitate pulverized-coal pyrolysis. The effects of the carrier-phase velocity are twofold: on one hand, a higher carrier-phase velocity will enhance the pyrolysis rate of coal particles; on the other hand, it will decrease the volatile concentration, which makes the ignition and combustion to be more difficult in a PCC case.

Extending the developed online-CPD-coupled LES approach to LES of pulverized-coal combustion is the objective of our research work in the next stage. The partially stirred reactor

(PaSR) model adapted for LES (Berglund et al., 2010) will be used to model the combustion of the 7 volatile species obtained in the online-CPD-coupled LES approach.

Acknowledgements

This work was supported by the National Basic Research Program of China (2012CB214906) and National Natural Science Foundation of China (51390491, 51422605). Kaidi Wan would like to acknowledge the financial support from the China Scholarship Council and the Engineering and Physical Sciences Research Council (EPSRC) of the UK. This work used the ARCHER UK National Supercomputing Service (<http://www.archer.ac.uk>).

Nomenclature

A_{tar} pre-exponential factor for tar cracking reaction, s^{-1}

A_v pre-exponential factor for conventional pyrolysis model, s^{-1}

$C_{p,g}$ specific heat capacity of the gas, $J/(kg \cdot K)$

$C_{p,p}$ specific heat capacity of a pulverized-coal particle, $J/(kg \cdot K)$

d	diameter, m
D	nozzle diameter, m
D_{diff}	molecular mass diffusion coefficient, m^2/s
E_p	equivalent emission of the particles in the local control volume, W/m^3
E_{tar}	activation energy for tar cracking reaction, J/mol
E_v	activation energy for conventional pyrolysis model, J/mol
f	drag coefficient of a pulverized-coal particle
G	incident radiation, W/m^2
I	radiation intensity, $W/(m^2 \cdot sr)$
k	absorption coefficient, m^{-1}

K_v	pyrolysis rate coefficient, s^{-1}
Le	Lewis number
m_v	mass of the volatile yields at current time step, kg
m_v^*	mass of the final volatile yields, kg
$m_v^{*'} $	mass of the volatile matter in proximate analysis, kg
$m_{Y,n}$	mass of the n th chemical species yields at current time step, kg
Nu	Nusselt number
p	pressure, Pa
Pr	Prandtl number
Q	Q-factor

Q_{conv}	convective heat transfer between the gas phase and a particle, W
Q_{rad}	heat transfer due to radiation, W
Q_{dev}	heat transfer due to pyrolysis (devolatilization), W
$q_{sgs,mom}$	subgrid-scale (SGS) term in momentum equation, $\text{kg}/(\text{m s}^2)$
$q_{sgs,Y}$	subgrid-scale (SGS) term in species equation, $\text{kg}/(\text{m}^2 \text{ s})$
$q_{sgs,T}$	subgrid-scale (SGS) term in energy equation, $\text{kg K}/(\text{m}^2 \text{ s})$
r	radial distance from the centerline, m
\vec{r}	position vector in radiative transfer equation (RTE), m
R	gas constant, $\text{J}/(\text{mol}\cdot\text{K})$
Re	Reynolds number

\bar{s}	outgoing direction of radiation
\bar{s}'	incoming direction of radiation
S_m	source term in mass equation, kg/(m ³ s)
S_{mom}	source term in momentum equation, kg/(m ² s ²)
S_Y	source term in species equation, kg/(m ³ s)
S_T	source term in energy equation, kg K/(m ³ s)
t	time, s
T	temperature, K
u	velocity, m/s
$U_{p,r}$	inlet velocity of particles at a radial distance of r from the centerline, m/s

$U_{p,c}$ inlet velocity of particles at the centerline, m/s

V_{cv} volume of the local control volume (cell), m³

W molar mass, kg/mol

x coordinate, m

X molar fraction, mol/mol

Y mass fraction, kg/kg

Greek symbols

ρ density, kg/m³

ω chemical reaction rate, mol/(m³ s)

ω_Y	chemical reaction source term in species equation, $\text{kg}/(\text{m}^3 \text{ s})$
ω_T	chemical reaction source term in energy equation, $\text{kg K}/(\text{m}^3 \text{ s})$
Δh_{dev}	heat of pyrolysis (devolatilization) reaction, J/kg
σ	Stefan-Boltzmann constant, $\text{W}/(\text{m}^2 \cdot \text{K}^4)$
σ_p	equivalent scattering coefficient of the particles in the control volume, m^{-1}
ε	emissivity
α	molecular thermal diffusivity coefficient, m^2/s
τ_{chem}	chemical time scale, s
τ_{ij}	viscous stress tensor in the momentum equation, $\text{kg}/(\text{m s}^2)$
τ_K	Kolmogorov time scale, s

τ_{Δ} characteristic time scale of the subgrid velocity stretch, s

τ_p response time of a pulverized-coal particle, s

τ_{sgs} subgrid turbulence time scale, s

δ_{ij} the Kronecker delta

μ molecular viscosity, Pa·s

ν molar stoichiometric coefficient

Φ scattering phase function

Ω' solid angle, sr

Subscripts

b	the blowing effects of a pulverized-coal particle
i, j, k	directions of the Cartesian coordinate
m	mass
mom	momentum
n	the n th chemical species
p	particle
R	radiation
sl	the velocity slip between the gas phase and a pulverized-coal particle

Operators

- spatial filtering
- density-weighted spatial filtering

References

- Al-Abbas, A.H., Naser, J., and Hussein, E.K. 2013. Numerical simulation of brown coal combustion in a 550 MW tangentially-fired furnace under different operating conditions. *Fuel*, **107**, 688-698.
- Badzioch, S., and Hawksley, P.G.W. 1970. Kinetics of thermal decomposition of pulverized coal particles. *Ind. Eng. Chem. Proc. Des. Dev.*, **9**(4), 521-530.
- Berglund, M., Fedina, E., Fureby, C., Tegnér, J., and Sabel'nikov, V. 2010. Finite Rate Chemistry Large-Eddy Simulation of Self-Ignition in Supersonic Combustion Ramjet. *AIAA J.*, **48**(3), 540-550.
- Bermúdez, A., Ferrín, J.L., Liñán, A., and Saavedra, L. 2011. Numerical simulation of group combustion of pulverized coal. *Combust. Flame*, **158**(9), 1852-1865.

Bu, C., Leckner, B., Chen, X., Pallarès, D., Liu, D., and Gómez-Barea, A. 2015. Devolatilization of a single fuel particle in a fluidized bed under oxy-combustion conditions. Part A: Experimental results. *Combust. Flame*, **162**(3), 797-808.

Chandrasekhar, S. 1960. *Radiative transfer*, Dover Publications, New York.

Chen, L., and Ghoniem, A.F. 2012. Simulation of oxy-coal combustion in a 100 kWth test facility using RANS and LES: a validation study. *Energy Fuels*, **26**(8), 4783-4798.

Cheng, Y., Xu, L., Li, X., and Chen, L. 2015. Online Estimation of Coal Calorific Value from Combustion Radiation for Coal-Fired Boilers. *Combust. Sci. Technol.*, **187**(10), 1487-1503.

Crowe, C.T., Sharma, M.P., and Stock, D.E. 1977. The particle-source-in cell (PSI-CELL) model for gas-droplet flows. *J. Fluids Eng.*, **99**(2), 325-332.

Devanathan, N., and Saxena, S.C. 1987. Transport model for devolatilization of large nonplastic coal particles: the effect of secondary reactions. *Ind. Eng. Chem. Res.*, **26**(3), 539-548.

Edge, P., Gubba, S.R., Ma, L., Porter, R., Pourkashanian, M., and Williams, A. 2011. LES modelling of air and oxy-fuel pulverised coal combustion—impact on flame properties. *Proc. Combust. Inst.*, **33**(2), 2709-2716.

Fairweather, M., and Hurn, J.P. 2008. Validation of an anisotropic model of turbulent flows containing dispersed solid particles applied to gas–solid jets. *Comput. Chem. Eng.*, **32**(3), 590-599.

- Fiveland, W.A. 1988. Three-dimensional radiative heat-transfer solutions by the discrete-ordinates method. *J. Thermophys. Heat Transf.*, **2**(4), 309-316.
- Fleckhaus, D., Hishida, K., and Maeda, M. 1987. Effect of laden solid particles on the turbulent flow structure of a round free jet. *Exp. Fluids*, **5**(5), 323-333.
- Fletcher, T.H., Kerstein, A.R., Pugmire, R.J., Solum, M.S., and Grant, D.M. 1992. Chemical Percolation Model for Devolatilization .3. Direct Use of C-13 Nmr Data to Predict Effects of Coal Type. *Energy Fuels*, **6**(4), 414-431.
- Franchetti, B.M., Cavallo Marincola, F., Navarro-Martinez, S., and Kempf, A.M. 2013. Large eddy simulation of a pulverised coal jet flame. *Proc. Combust. Inst.*, **34**(2), 2419-2426.
- Genetti, D., Fletcher, T.H., and Pugmire, R.J. 1999. Development and application of a correlation of ¹³C NMR chemical structural analyses of coal based on elemental composition and volatile matter content. *Energy Fuels*, **13**(1), 60-68.
- Genetti, D.B. 1999. *An advanced model of coal devolatilization based on chemical structure*. M.S. Thesis, Brigham Young University, Provo, Utah, USA.
- Germano, M., Piomelli, U., Moin, P., and Cabot, W.H. 1991. A dynamic subgrid - scale eddy viscosity model. *Phys. Fluids A*, **3**(7), 1760-1765.

Gharebaghi, M., Irons, R.M.A., Ma, L., Pourkashanian, M., and Pranzitelli, A. 2011. Large eddy simulation of oxy-coal combustion in an industrial combustion test facility. *Int. J. Greenh. Gas Control*, **5**, S100-S110.

Grant, D.M., Pugmire, R.J., Fletcher, T.H., and Kerstein, A.R. 1989. Chemical-Model of Coal Devolatilization Using Percolation Lattice Statistics. *Energy Fuels*, **3**(2), 175-186.

Hashimoto, N., Kurose, R., Hwang, S.M., Tsuji, H., and Shirai, H. 2012. A numerical simulation of pulverized coal combustion employing a tabulated-devolatilization-process model (TDP model). *Combust. Flame*, **159**(1), 353-366.

Hwang, S.M., Kurose, R., Akamatsu, F., Tsuji, H., Makino, H., and Katsuki, M. 2005. Application of optical diagnostics techniques to a laboratory-scale turbulent pulverized coal flame. *Energy Fuels*, **19**(2), 382-392.

Jiang, X., Siamas, G.A., Jagus, K., and Karayiannis, T.G. 2010. Physical modelling and advanced simulations of gas-liquid two-phase jet flows in atomization and sprays. *Prog. Energy Combust. Sci.*, **36**(2), 131-167.

Jones, W.P., Lyra, S., and Navarro-Martinez, S. 2011. Large Eddy Simulation of a swirl stabilized spray flame. *Proc. Combust. Inst.*, **33**(2), 2153-2160.

- Kuang, M., Wang, Z., Zhu, Y., Ling, Z., and Li, Z. 2014. Regulating Low-NO_x and High-Burnout Deep-Air-Staging Combustion under Real-Furnace Conditions in a 600 MWe Down-Fired Supercritical Boiler by Strengthening the Staged-Air Effect. *Environ. Sci. Technol.*, **48**(20), 12419-12426.
- Kurose, R., and Makino, H. 2003. Large eddy simulation of a solid-fuel jet flame. *Combust. Flame*, **135**(1–2), 1-16.
- Kurose, R., Watanabe, H., and Makino, H. 2009. Numerical simulations of pulverized coal combustion. *KONA Powder Part. J.*, **27**, 144-156.
- Lilly, D.K. 1992. A proposed modification of the Germano subgrid - scale closure method. *Phys. Fluids A*, **4**(3), 633-635.
- Liu, X.D., Osher, S., and Chan, T. 1994. Weighted essentially non-oscillatory schemes. *J. Comput. Phys.*, **115**(1), 200-212.
- Liu, Y., and He, R. 2015. Modeling of the Pore Structure Evolution in Porous Char Particles During Combustion. *Combust. Sci. Technol.*, null-null.
- Lu, H., Ip, E., Scott, J., Foster, P., Vickers, M., and Baxter, L.L. 2010. Effects of particle shape and size on devolatilization of biomass particle. *Fuel*, **89**(5), 1156-1168.

Lv, Y., Wang, Z., Zhou, J., and Cen, K. 2010. Full-scale numerical investigation of a selective noncatalytic reduction (SNCR) system in a 100 MW utility boiler with complex chemistry and decoupling approach. *Energy Fuels*, **24**(10), 5432-5440.

Miller, R.S., and Bellan, J. 1999. Direct numerical simulation of a confined three-dimensional gas mixing layer with one evaporating hydrocarbon-droplet-laden stream. *J. Fluid Mech.*, **384**, 293-338.

Mittal, V., and Pitsch, H. 2013. A flamelet model for premixed combustion under variable pressure conditions. *Proc. Combust. Inst.*, **34**(2), 2995-3003.

Modest, M.F. 2013. *Radiative heat transfer*, third ed., Academic Press, New York.

Moin, P., Squires, K., Cabot, W., and Lee, S. 1991. A dynamic subgrid - scale model for compressible turbulence and scalar transport. *Phys. Fluids A*, **3**(11), 2746-2757.

Pedel, J., Thornock, J.N., and Smith, P.J. 2012. Large eddy simulation of pulverized coal jet flame ignition using the direct quadrature method of moments. *Energy Fuels*, **26**(11), 6686-6694.

Pierce, C.D., and Moin, P. 1998. Method for generating equilibrium swirling inflow conditions. *AIAA J.*, **36**(7), 1325-1327.

Poinsot, T., and Veynante, D. 2012. *Theoretical and numerical combustion*, third ed., Aquaprint, Bordeaux, France.

- Prüfert, U., Hunger, F., and Hasse, C. 2014. The analysis of chemical time scales in a partial oxidation flame. *Combust. Flame*, **161**(2), 416-426.
- Rabacal, M., Franchetti, B.M., Marincola, F.C., Proch, F., Costa, M., Hasse, C., and Kempf, A.M. 2015. Large eddy simulation of coal combustion in a large-scale laboratory furnace. *Proc. Combust. Inst.*, **35**(3), 3609-3617.
- Ranz, W.E., and Marshall, W.R. 1952. Evaporation from drops. *Chem. Eng. Prog.*, **48**(3), 141-146.
- Schlüter, J.U., Pitsch, H., and Moin, P. 2004. Large-eddy simulation inflow conditions for coupling with Reynolds-averaged flow solvers. *AIAA J.*, **42**(3), 478-484.
- Stöllinger, M., Naud, B., Roekaerts, D., Beishuizen, N., and Heinz, S. 2013. PDF modeling and simulations of pulverized coal combustion – Part 2: Application. *Combust. Flame*, **160**(2), 396-410.
- Stein, O.T., Olenik, G., Kronenburg, A., Marincola, F.C., Franchetti, B.M., Kempf, A.M., Ghiani, M., Vascellari, M., and Hasse, C. 2013. Towards comprehensive coal combustion modelling for LES. *Flow Turbul. Combust.*, **90**(4), 859-884.
- Ströhle, J., Chen, X., Zorbach, I., and Epple, B. 2014. Validation of a Detailed Reaction Mechanism for Sulfur Species in Coal Combustion. *Combust. Sci. Technol.*, **186**(4-5), 540-551.

Sutherland, W. 1893. LII. The viscosity of gases and molecular force. *Philos. Mag.*, **36**(223), 507-531.

Taniguchi, M., Okazaki, H., Kobayashi, H., Azuhata, S., Miyadera, H., Muto, H., and Tsumura, T. 2001. Pyrolysis and ignition characteristics of pulverized coal particles. *J. Energy Resour. Technol.*, **123**(1), 32-38.

Truelove, J.S. 1987. Discrete-ordinate solutions of the radiation transport equation. *J. Heat Transfer*, **109**(4), 1048-1051.

Vascellari, M., Arora, R., Pollack, M., and Hasse, C. 2013a. Simulation of entrained flow gasification with advanced coal conversion submodels. Part 1: Pyrolysis. *Fuel*, **113**, 654-669.

Vascellari, M., and Cau, G. 2012. Influence of turbulence–chemical interaction on CFD pulverized coal MILD combustion modeling. *Fuel*, **101**, 90-101.

Vascellari, M., Xu, H., and Hasse, C. 2013b. Flamelet modeling of coal particle ignition. *Proc. Combust. Inst.*, **34**(2), 2445-2452.

Wan, K.D., Wang, Z.H., He, Y., Xia, J., Zhou, Z.J., Zhou, J.H., and Cen, K.F. 2015. Experimental and modeling study of pyrolysis of coal, biomass and blended coal–biomass particles. *Fuel*, **139**, 356-364.

- Wang, Z.H., Wan, K.D., Xia, J., He, Y., Liu, Y.Z., and Liu, J.Z. 2015. Pyrolysis Characteristics of Coal, Biomass, and Coal–Biomass Blends under High Heating Rate Conditions: Effects of Particle Diameter, Fuel Type, and Mixing Conditions. *Energy Fuels*, **29**(8), 5036-5046.
- Xia, J., Luo, K.H., and Kumar, S. 2008. Large-Eddy Simulation of Interactions Between a Reacting Jet and Evaporating Droplets. *Flow Turbul. Combust.*, **80**(1), 133-153.
- Xia, J., Luo, K.H., and Zhao, H. 2011. Dynamic Large-Eddy Simulation of Droplet Effects on a Reacting Plume in Countercurrent Configuration. *Combust. Sci. Technol.*, **183**(5), 487-518.
- Xia, J., Zhao, H., Megaritis, A., Luo, K.H., Cairns, A., and Ganippa, L.C. 2013. Inert-droplet and combustion effects on turbulence in a diluted diffusion flame. *Combust. Flame*, **160**(2), 366-383.
- Xu, L., Kang, Y., Zhang, G., Wang, T., and Wu, T. 2015. Study of Alkali Emission and Control with Firing a High Alkali Coal. *Combust. Sci. Technol.*, **187**(12), 1959-1973.
- Yamamoto, K., Murota, T., Okazaki, T., and Taniguchi, M. 2011. Large eddy simulation of a pulverized coal jet flame ignited by a preheated gas flow. *Proc. Combust. Inst.*, **33**(2), 1771-1778.
- Yi, F.X. 2012. *Direct Numerical Simulation of Gas/Coal Particles Gas-Solid Two-Phase Round Jet Combustion Flow*. Ph.D. Thesis, Zhejiang University, Hangzhou, China (in Chinese).
- Zhao, X.Y., and Haworth, D.C. 2014. Transported PDF modeling of pulverized coal jet flames. *Combust. Flame*, **161**(7), 1866-1882.

Table 1. Proximate and ultimate analysis of coals.

Coal	Yallourn (YL)	Vicary Creek (VC)	Hongay (HG)
<i>Proximate analysis (dry basis, wt%)</i>			
Volatile matter	53.3	21.7	7.3
Fixed carbon	45.5	66.0	88.2
Ash	1.2	12.4	4.5
<i>Ultimate analysis (daf basis, wt%)</i>			
C	65.4	87.8	93.7
H	4.9	4.7	3.3
N	0.6	2.1	1.2
S	0.3	0.4	0.8

0	28.8	4.9	1.3
---	------	-----	-----

Accepted Manuscript

Table 2. Structural parameters of the CPD model.

Structural parameter	Yallourn (YL)	Vicary Creek (VC)	Hongay (HG)
MW_{δ}	50	21	9
MW_{cl}	340	267	249
p_0	0.68	0.67	0.92
$\sigma + 1$	4.1	4.6	3.8
c_0	0.15	0.23	0.36

Table 3. Simulation cases and parameters.

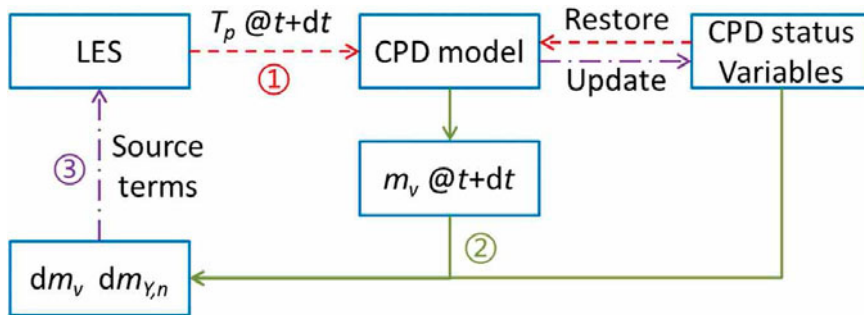
Cases	Parameters	Setup
A	(Baseline case)	<p>(1) Pyrolysis model: online CPD model;</p> <p>(2) Particle size distribution: $d_{p,mean} = 45 \mu\text{m}$, $d_{p,sd} = 120 \mu\text{m}$ (log-normal);</p> <p>(3) Coal type: Vicary Creek;</p> <p>(4) Coal-feeding rate: $5.1 \times 10^{-4} \text{ kg/s}$;</p> <p>(5) Carrier-phase velocity: 10 m/s;</p> <p>(6) Co-flow temperature: 2000 K.</p>
AA	Pyrolysis model	SFOM
B1	Particle size distribution	$d_{p,mean} = 22.5 \mu\text{m}$, $d_{p,sd} = 10 \mu\text{m}$ (log-normal)
B2	Particle size distribution	$d_{p,mean} = 90 \mu\text{m}$, $d_{p,sd} = 10 \mu\text{m}$ (log-normal)

C1	Coal type	Yallourn (higher volatile content)
C2	Coal type	Hongay (lower volatile content)
D1	Coal-feeding rate	Double the value of the baseline Case A
D2	Coal-feeding rate	Half the value of the baseline Case A
E	Carrier-phase velocity	Double the value of the baseline Case A
F	Co-flow temperature	1600 K

Table 4. Average wall-clock-time per time step

	Conventional-LES	CPD-LES
Total (s)	5.95	9.01
<i>Time consumed by different modules</i>		
Scalar transport equations (s)	0.38	1.47
Particle transport equations (s)	1.03	2.28
Others (s)	4.54	5.26

Figure 1. Coupling the CPD model into an LES solver.



Accepted Manuscript

Figure 2. Comparison of the radial profiles of the gas and particle phase statistics: (a-b) mean axial velocity, (c-d) turbulence kinetic energy, and (e-f) shear stress, at 3 downstream locations, i.e., $x/D = 10, 20$ and 30 . The experimental data (Fleckhaus et al., 1987), Reynolds-stress model predictions (Fairweather and Hurn, 2008), $k-\varepsilon$ model predictions (Fairweather and Hurn, 2008) and large-eddy simulation predictions are denoted by “exp”, “RS”, “ $k-\varepsilon$ ”, and “LES”, respectively.

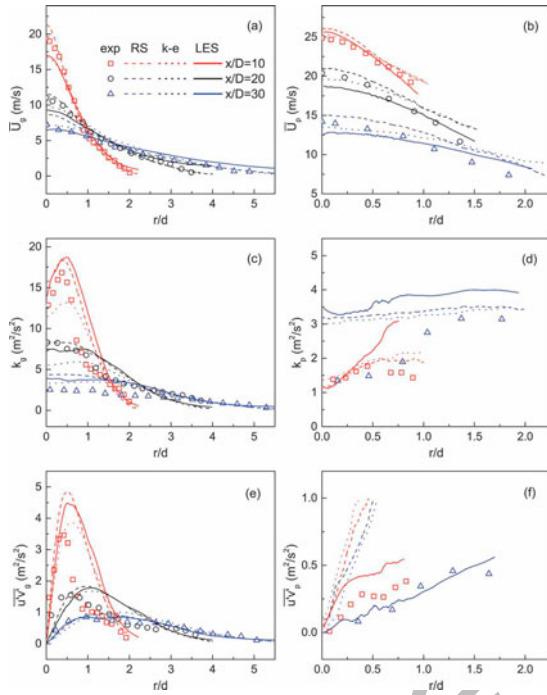
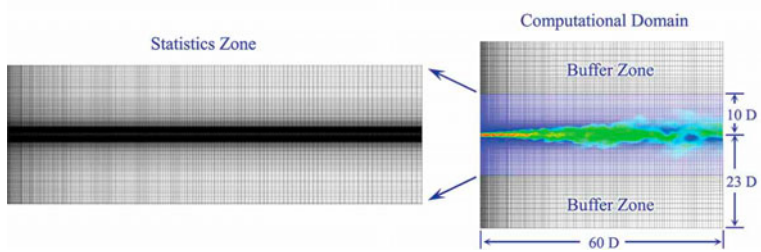


Figure 3. Computational domain and grid distribution.



Accepted Manuscript

Figure 4. Instantaneous pulverized-coal particle distribution and the $Y_{CH_4} = 0.25\%$ iso-surface, which is colored by gas temperature. CH_4 is one of the major volatile species. The pulverized-coal particles are colored by the particle density, which denotes the instantaneous particle mass. The size of the coal particles is also illustrated in the figure. The IVZ, GV, and CV denote the isolated, growing, and continuous volatile zones, respectively.

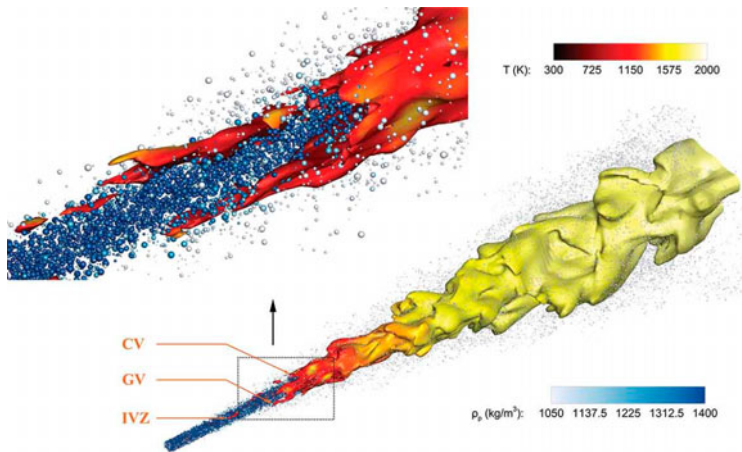


Figure 5. Instantaneous particle pyrolysis scatter plot for the four particle diameter sections: (a-d) CPD-LES and (e-h) Conventional-LES.

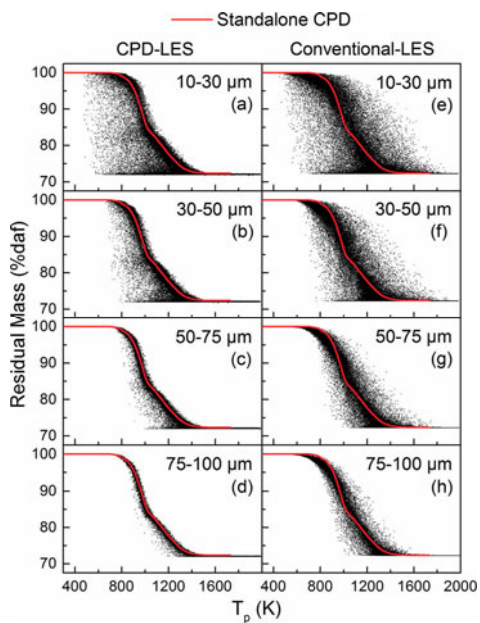


Figure 6. Comparison of an instantaneous particle pyrolysis scatter plot between the (a) CPD-LES and (b) Conventional-LES predictions.

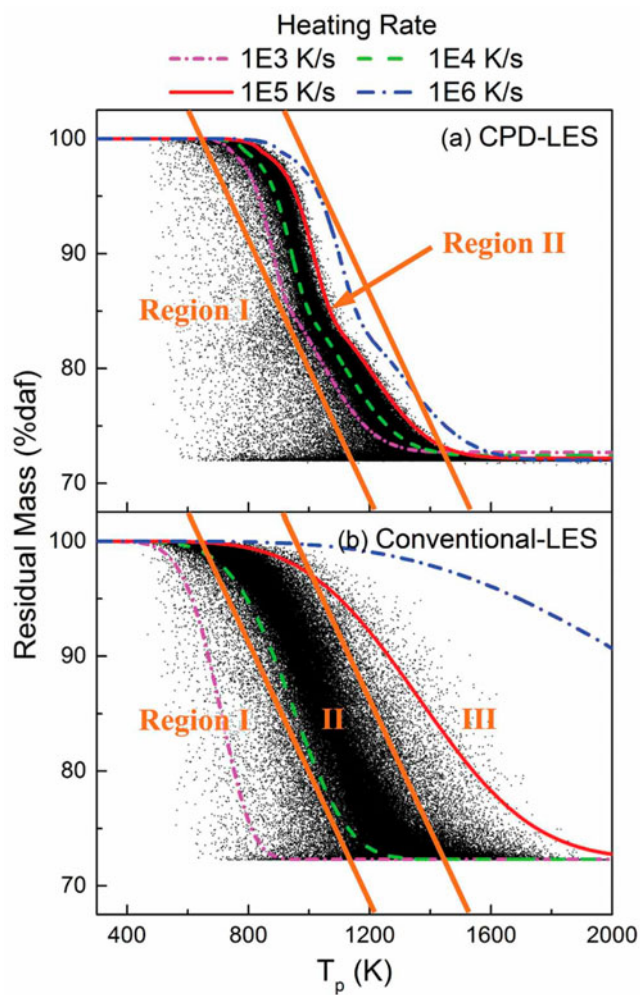


Figure 7. Scatter plot of the normalized instantaneous particle pyrolysis rate against particle temperature for the particles experiencing a high heating rate ($> 1 \times 10^5$ K/s) in the (a) CPD-LES and (b) Conventional-LES.

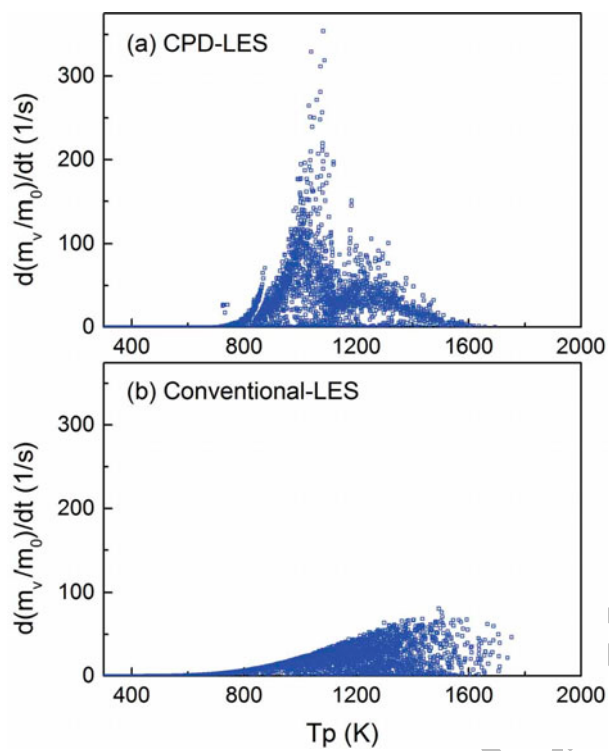
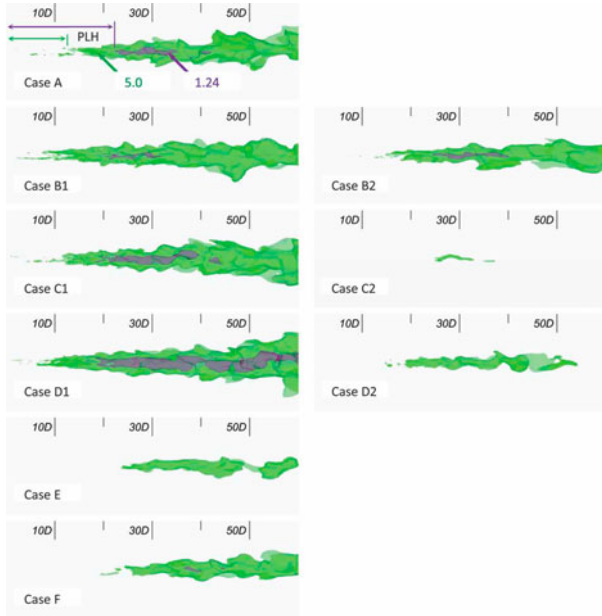


Figure 8. The iso-surfaces of $SR_g = 1.24$ and 5.0 predicted by the online-CPD-coupled LES.



Accepted Manuscript

Figure 9. Pyrolysis lift-off heights defined by $SR_g = 1.24$ and 5.0 and predicted by the online-CPD-coupled LES.

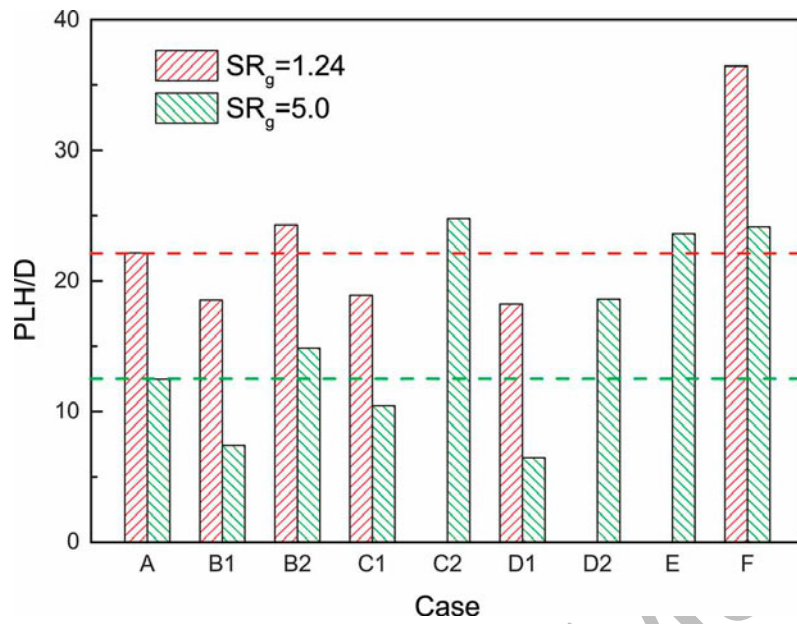


Figure 10. The normalized instantaneous pyrolysis rate of pulverized-coal particles predicted by the online-CPD-coupled LES.

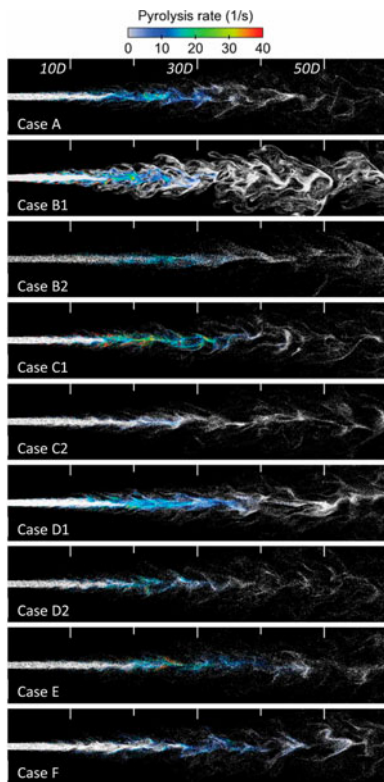
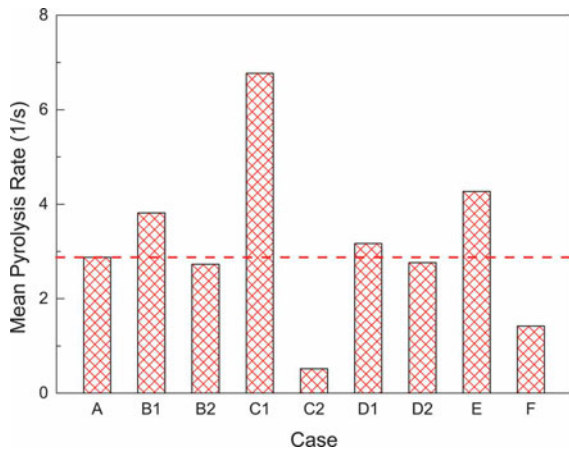


Figure 11. The mean pyrolysis rate of all pulverized-coal particles for which the pyrolysis rate is not zero in the computational domain predicted by the online-CPD-coupled LES.



Color figures can be used for the online PDF version and the gray style for hardcopy reproduction.